

Non-Gaussian mechanical motion via single and multi-phonon subtraction from a thermal state

G. Enzian^{†, 1, 2, 3} L. Freisem^{†, 1, 2} J. J. Price^{†, 1, 2} A. Ø. Svela^{†, 1, 2, 4} J. Clarke,¹
B. Shajilal,⁵ J. Janousek,⁵ B. C. Buchler,⁵ P. K. Lam,⁵ and M. R. Vanner^{1, 2, *}

¹*QOLS, Blackett Laboratory, Imperial College London, London SW7 2BW, United Kingdom*

²*Clarendon Laboratory, Department of Physics, University of Oxford, Oxford OX1 3PU, United Kingdom*

³*Niels Bohr Institute, University of Copenhagen, Copenhagen 2100, Denmark*

⁴*Max Planck Institute for the Science of Light, Staudtstraße 2, 91058 Erlangen, Germany*

⁵*Centre for Quantum Computation and Communication Technology,*

Research School of Physics and Engineering, Australian National University, Canberra 2601, Australia

(Dated: Latest revision: March 1, 2025)

Quantum optical measurement techniques offer a rich avenue for quantum control of mechanical oscillators via cavity optomechanics. In particular, a powerful yet little explored combination utilizes optical measurements to perform heralded non-Gaussian mechanical state preparation and to determine the mechanical phase-space distribution. Here, we experimentally perform heralded single- and multi-phonon subtraction via photon counting to a room temperature mechanical thermal state with a Brillouin optomechanical system, and use optical heterodyne detection to measure the s -parameterized Wigner phase-space distribution of the non-Gaussian mechanical states generated. The techniques developed here will be useful for a broad range of both applied and fundamental studies that exploit quantum-state engineering and reconstruction of mechanical motional states.

Introduction.—A key current goal in cavity quantum optomechanics is to generate and reconstruct non-Gaussian states of mechanical motion that exhibit non-classical behavior. Pursuing this line of research will facilitate the development of mechanical-oscillator-based quantum technology components such as quantum memories exploiting the long coherence times available [1–3], coherent transducers [4, 5], and sensors [6–8]. Additionally, such state generation and reconstruction capabilities will help enable tests of fundamental physics including exploring the quantum-to-classical transition [9–11] and even studying the interface between quantum mechanics and gravity [12–14].

Throughout the other facets of quantum optics, non-Gaussian state preparation of a bosonic mode followed by phase-space reconstruction has been performed with a wide spectrum of different experimental platforms. As an early notable example, a single-phonon Fock state of motion of a trapped ion was prepared and reconstructed [15], and further work with trapped-ions has generated multi-component superposition states of motion for quantum-information applications [16]. In optics, heralded single-photon addition and subtraction followed by homodyne tomography has been utilized to generate and reconstruct several different quantum states that are now being explored for quantum science and technology applications. For instance, the Wigner function of a heralded single-photon state has been reconstructed [17], single-photon subtraction to squeezed states has been performed to generate small superposition states [18, 19], which have a superposition separation size that is enhanced by multi-phonon subtraction [20], and the non-Gaussianity of photon-added and photon-subtracted thermal states has been studied [21–23]. Other notable examples of non-Gaussian quantum

states with other physical systems include: studying the decoherence of a superposition state of a microwave field inside a cavity [24], generating non-Gaussian states of atomic-spin ensembles [25], creating and reconstructing arbitrary quantum states in a microwave superconducting circuit [26], and creating non-classical states of high-frequency acoustic waves coupled to superconducting qubits [27, 28].

Within optomechanics there have been several recent developments in this direction, with many experimental approaches being utilized to take advantage of the parameters and capabilities provided by fully engineered optomechanical devices. For instance, experiments exploiting quantum measurements with single-photon detectors include generating non-classical states of high-frequency vibrations in diamond crystals [29–31] and photonic-crystal structures [32], second-order-coherence measurements of mechanical modes [33, 34], the generation of mechanical interference fringes [40], and single-phonon addition or subtraction to a thermal state that results in a doubling of the mean thermal occupation [35]. There is also significant progress towards developing the experimental tools needed for mechanical phase-space tomography or reconstruction [36–40]; however, all of these experiments have insufficient sensitivity to resolve features below the mechanical zero-point motion, and phase-space tomography or reconstruction [41] of a mechanical quantum state remains as an outstanding goal in optomechanics. One promising route to achieving this goal in the resolved sideband regime is to perform single-phonon addition or subtraction for quantum state preparation and then utilize a red-sideband drive and optical state tomography with a balanced detector, such as homodyne or heterodyne detection.

* www.qmeas.net (m.vanner@imperial.ac.uk)

In this Letter, we report an experimental study that performs single- and multi-phonon subtraction operations to a thermal state of a mechanical oscillator to create non-Gaussian states of motion. These operations are heralded by single- and multi-photon detection events following an optomechanical interaction at room temperature and we utilize quantum-noise-limited heterodyne detection to characterize the phase space of the mechanical states prepared. We observe that the initial thermal state is transformed by these operations from an initial Gaussian in phase space into a ring shape with a diameter that increases with the number of phonons subtracted. Building on established results in quantum optics and recent work demonstrating that the mechanical mean thermal occupation doubles for single-phonon addition and subtraction [35], here we also observe that the mean thermal occupation triples for two-phonon subtraction. This work expands the toolkit for optical control and readout of mechanical states, and can be applied to future room-temperature or cryogenic experiments to exploit and characterize the non-Gaussian and non-classical properties these operations generate.

Multi-phonon addition and subtraction scheme.—To perform n -phonon addition or subtraction, we use a pair of optical modes of an optical cavity that are approximately spaced by the mechanical frequency (cf. Fig. 1(a)) to resonantly enhance the optomechanical interaction. Each optical mode also has a linewidth much narrower than the mechanical frequency allowing operation deeply within the resolved sideband regime. By optically driving the lower-frequency mode of the pair, the anti-Stokes scattering process is selected and a signal field in the higher-frequency cavity mode is generated. This scattering process is described by a light-mechanics beamsplitter-type interaction with Hamiltonian $H/\hbar = G(a^\dagger b + ab^\dagger)$, where G is the pump-enhanced linearized optomechanical coupling rate, a is the field operator of the optical signal field, and b is the mechanical annihilation operator. Then, for weak optomechanical coupling, detecting n signal photons heralds an n -phonon subtraction operation to the mechanical state. For an initial mechanical thermal state $\rho_{\bar{n}}$, with mean thermal occupation \bar{n} , the mechanical state following this operation can be determined via $\rho_{n-} \propto b^n \rho_{\bar{n}} b^{\dagger n}$. In a similar manner, by optically driving the upper-frequency mode of the pair, the Stokes scattering process is selected ($H/\hbar = G(ab + a^\dagger b^\dagger)$) and detecting n photons in the frequency down shifted Stokes signal heralds an n -phonon addition process, $\rho_{n+} \propto b^{\dagger n} \rho_{\bar{n}} b^n$. These operations are a multi-phonon generalization to the single-phonon addition and subtraction operations considered in Ref. [42].

When performing single- or multi-phonon subtraction or addition to a thermal state of large mean thermal occupation, one may expect very little change to the mechanical motional state. However, these operations significantly change the mean occupation and give rise to highly non-Gaussian distributions in mechanical phase space. Indeed, when applying an n -fold subtraction operation, the mean occupation transforms via $\bar{n} \rightarrow (n+1)\bar{n}$, and for n -fold addition $\bar{n} \rightarrow (n+1)\bar{n} + n$. For $\bar{n} \gg 1$, it is noted that the mean occupation *doubles* for single-quanta addition or

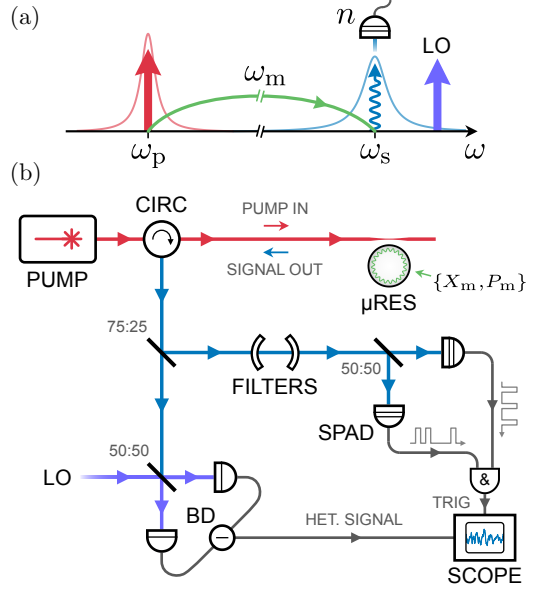


FIG. 1. Multi-phonon subtraction scheme and experimental setup. (a) Optical pumping and heralding scheme. A pair of optical resonances spaced by the mechanical angular frequency ω_m are used to resonantly enhance the optomechanical interaction. Here, a pump field drives a mode at ω_p creating an anti-Stokes signal at ω_s . An n -phonon detection scheme is then used to herald n -phonon subtraction to the mechanical motion. Swapping the roles of pump and detection can be used for n -phonon addition. (b) Experimental schematic. A pump laser drives an optical microresonator and the backscattered anti-Stokes signal is separated from the pump with an optical circulator (CIRC). The signal is subsequently split and detected via single photon avalanche detectors (SPADs) to herald a single- or two-phonon subtraction operation. To characterize the mechanical state prepared, heterodyne detection is performed (BD: balanced detector, LO: local oscillator), and the signal recorded on an oscilloscope triggered by SPAD detection events. The two-phonon subtraction case is shown here that uses a two-photon-coincidence measurement.

subtraction—which has been experimentally observed for thermal optical fields [21] and very recently for a mechanical thermal state [35]—and the mean occupation *triples* for two-quanta addition or subtraction. This significant change to the mean occupation and the non-Gaussian ring shape observed in phase space can be understood via a combination of the shift to the probability distribution of the number operator and the Bayesian inference of the non-unitary quantum-measurement process [43]. The mechanical states created by these operations are phase-invariant since the initial thermal state is phase-invariant, and the optomechanical interactions, as well as the addition and subtraction operations, also preserve the mechanical phase-independence. It is also important to note that in the limit $\bar{n} \gg \sqrt{n}$ the mechanical state generated by an n -phonon addition to a thermal state is the same as that generated by an n -phonon subtraction operation. Thus, for this work, we focus on n -phonon subtraction and mechanical state readout using the anti-Stokes interaction as, in contrast to the Stokes process, the anti-Stokes process is the best suited for mechanical state readout as it does not give rise to lasing

and instability for large drive strengths and the optical field is a high-fidelity proxy for the mechanical state in the limit of high efficiency. See the Supplementary Material [49] for a mathematical discussion of these states, the interactions used, and their properties.

Experimental setup.—In this work, n -phonon subtraction is experimentally implemented by driving anti-Stokes Brillouin scattering in a BaF₂ optical microresonator. The optical fiber-coupled microresonator, with optical quality factor $Q \simeq 10^8$, has a micro-rod-resonator geometry similar to that used in Ref. [35], with a major diameter and minor radius of curvature of 936 μm and $\sim 40 \mu\text{m}$, respectively.

To identify a suitable pair of optical resonances, a tunable continuous-wave laser at 1550 nm was evanescently coupled into the microresonator at low power and swept in wavelength (cf. Fig. 1(b)). Pairs of optical resonances separated by approximately the Brillouin shift can be identified and investigated for anti-Stokes Brillouin scattering by pumping on the lower-frequency optical mode of the pair. For the results presented in this Letter, a pump mode and an anti-Stokes mode with amplitude decay rates of $\kappa_1/2\pi = 7.1 \text{ MHz}$ and $\kappa_2/2\pi = 46.9 \text{ MHz}$, respectively, are used. The separation of the two optical modes was approximately equal to the measured mechanical frequency, $\omega_m/2\pi = 8.16 \text{ GHz}$. Furthermore, the mechanical amplitude decay rate and intrinsic optomechanical coupling rate were measured to be $\gamma/2\pi = 3.26(39) \text{ MHz}$ and $g_0/2\pi = 296(39) \text{ Hz}$, respectively (see Supplementary Material [49] for further details). The experiment was performed at 300 K, corresponding to a mean thermal occupation of the mechanical mode of $\bar{n}_{\text{th}} \simeq 766$, which, via the optomechanical coupling was sideband-cooled to $\bar{n} \simeq 453(52)$ before single- or multi-phonon subtraction occurs. To drive the anti-Stokes interaction, the laser is locked on-resonance to the pump mode using Pound–Drever–Hall frequency stabilization. An input pump power of $\sim 9 \text{ mW}$ was used, corresponding to an intra-cavity pump photon number of $N_{\text{cav}} \simeq 1.2 \times 10^9$ and optomechanical coupling rate of $G/2\pi \simeq 10 \text{ MHz}$, such that the system is well within the weak coupling regime ($2G < \kappa + \gamma$). The backscattered anti-Stokes Brillouin light is coupled out of the cavity by a silica tapered fiber, with efficiency $\eta_c \simeq 0.25$, and is then separated from the forwards-propagating pump field using an optical circulator before being split into two arms using a 75:25 beamsplitter: one for heralding via photon counting and one for heterodyne detection.

In the 25% arm, single- and two-phonon subtraction events are heralded via single-photon detection using two single-photon avalanche detectors (SPAD). Prior to the detectors, two fiber-based Fabry–Perot filters are used in series to filter out deleterious photons from the pump-field. Using a 50 kHz gate, we observe a singles count rate of $280(40) \text{ s}^{-1}$ when splitting the signal onto both detectors. As the count rate is much greater than the dark count rate ($\sim 1 \text{ s}^{-1}$), and only the heralding probability is affected by optical losses in the system, the detection of single-photon and two-photon-coincidence events herald single- and two-phonon subtractions with high fidelity, respectively. Note that as the gate duration is much less than the decay time

$1/(\gamma + G^2/\kappa) \simeq 31 \text{ ns}$, the heralding of two-photon events is well approximated as simultaneous detections.

In the 75% arm, balanced heterodyne detection is performed to experimentally access the quadrature components of the conditioned mechanical states. The detection scheme is implemented by interfering the anti-Stokes signal and a strong local oscillator, that is frequency-detuned by $\omega_H/2\pi = 214 \text{ MHz}$ with respect to the signal, onto a 50:50 beamsplitter and measuring the output using a balanced photodetector. The two types of photon counting events—singles and two-photon coincidences—then trigger a high-bandwidth oscilloscope to record a time-trace of the output from the balanced detector. In order to acquire sufficient statistics for the phase-space distributions and temporal dynamics of the mechanical states for the initial, single-phonon subtracted, and two-phonon subtracted thermal states, 2.4×10^5 time traces were recorded for each case.

Mechanical state readout.—A promising route to perform mechanical quantum state reconstruction is to use optical homodyne or heterodyne tomography, as utilized in quantum optics, after having performed an efficient transfer of the mechanical state to the optical field. In the absence of losses or inefficiencies, if optical homodyne tomography is performed after the state transfer, then the marginals obtained allow the mechanical Wigner function to be reconstructed. And, if a heterodyne measurement is performed instead, owing to the vacuum noise introduced with the simultaneous measurement of the two conjugate optical quadratures, the Husimi- Q function is then determined.

In practice, one of the most important aspects to such a measurement is the overall efficiency, as any loss and inefficiency reduces the quality of the phase-space distribution obtained. More specifically, optical losses result in the state of interest being convolved in phase space with vacuum noise, thus degrading the signal and even eliminating any non-classical features present if the efficiency is poor. This fact has been highlighted by many quantum optics experiments, and for instance, an overall efficiency of greater than 50% was required in Ref. [17] to see the Wigner negativity of a single-photon Fock state.

A versatile way to mathematically capture the effect of such losses is to use the s -parameterized Wigner function $W_s(X_m, P_m)$ [44]. For optical heterodyne detection, the s -parameter is defined as $s = (\eta - 2)/\eta$, where η is the overall measurement efficiency of the mechanical state including the mechanics-light transduction efficiency. From the expression for s , we can see that for $\eta = 1$ we have $s = -1$, which corresponds to the Q function, and for $\eta < 1$ we have $s < -1$ corresponding to a distribution that is smoothed more than the Q function. Experimentally determining W_s for mechanical states is valuable as it fully characterizes the state, allows any statistic or measurement probability to be determined, and will aid greatly in mechanical quantum state engineering research directions.

In this experiment, via the light-mechanics beam-splitter interaction of the anti-Stokes process, the scattered optical signal acts as a proxy for the mechanical state, and is used to characterize the mechanical state generated at the time

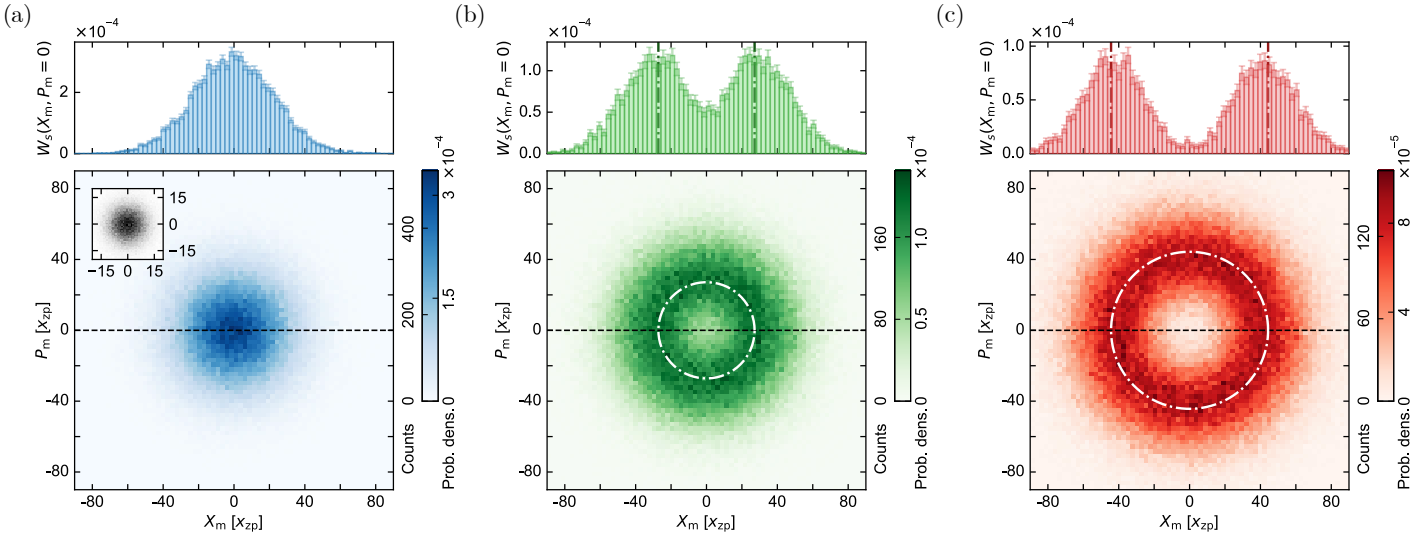


FIG. 2. Experimentally reconstructed s -parameterized Wigner functions W_s (bottom row), with slices through $P_m = 0$ (top row), for an (a) initial, (b) single-phonon subtracted and (c) two-phonon subtracted mechanical thermal state. The phase-space distributions are plotted in units of the mechanical zero-point fluctuations x_{zp} and are obtained through heterodyne detection of the optical anti-Stokes signal. The introduction of non-Gaussianity into the originally Gaussian phase-space distribution is observed for single-phonon subtraction, which further grows upon two-phonon subtraction. The dash-dotted lines indicate the theoretically predicted maxima for the W_s functions. The phase-space distribution (Husimi Q -function) of the optical vacuum contribution, where no optomechanical signal is present at the heterodyne detector, is shown in the inset in panel (a).

of the herald event. To extract the two orthogonal quadrature components from the heterodyne signal, we mix down the signal at the heterodyne frequency in post-processing for each herald event, and a two-dimensional histogram of the mechanical phase-space distribution W_s is formed.

Results and discussion.—The experimentally determined mechanical phase-space distributions W_s are plotted in Fig. 2 for the initial thermal state, the single-phonon subtracted state, and the two-phonon subtracted state. The measurement of the initial thermal state is useful to characterize the initial Gaussian state and to determine the overall efficiency of the measurement η . Since we are performing a heterodyne measurement, the variance of the quadrature component is $\sigma^2 = \eta\bar{n} + 1$ when the optical vacuum contribution is normalized to 1 [49]. We then determine an overall efficiency $\eta = 1.54\%$ via independent measurement of the optical vacuum, and knowledge of the initial thermal occupation ($\bar{n} = 453$ laser cooled). This efficiency yields an s -parameter of $s = -129$, indicating that the phase-space distribution determined is smoothed more than the Q function. Knowing η also allows working with units of the mechanical zero-point fluctuations x_{zp} simply by scaling the heterodyne signals accordingly. The experimentally determined phase-space distributions for the single- and two-phonon subtracted cases show the highly non-Gaussian ring shape, with increasing radius from one- to two-phonon subtraction. Theoretical predictions [49] for the radii of the phase-space rings are indicated by the dash-dotted lines in Fig. 2, which agree with the phase-space distributions W_s experimentally obtained.

Figure 3(a) shows the scaled heterodyne quadrature variance σ^2/η as a function of time about the herald event.

Note that the variance observed for the thermal state is equal to the sum of the initial thermal occupation $\bar{n} = 453$ and the added noise of $|s|/2 = 65$ mechanical quanta from the optical vacuum contribution. For the single- and two-phonon subtraction cases, it is observed that the variance increases at the time of the herald event and the ‘doubling’ and ‘tripling’ is observed for the two cases, respectively. At the herald-event time $t - t_0 = 0$, we observe that $\bar{n}_{1-}/\bar{n} = 1.94$ and $\bar{n}_{2-}/\bar{n} = 2.94$ in close agreement with the theoretical predictions [49] where only t_0 is a free fitting parameter (solid lines). We understand the small difference between our experimental observations and the theoretical prediction to be due to the filtering performed in the quadrature demodulation, the small level of dark counts in the SPAD detectors, and the optical filtering performed in the heralding arm.

With the mechanical phase-space distributions, the expectation value of any observable can then be readily computed. In Fig. 3(b), we have plotted the X_m quadrature marginals $\text{Pr}(X_m) = \int_{-\infty}^{\infty} dP_m W_s(X_m, P_m)$ as a function of time about the herald event. This plot illustrates how the state transforms by the single- and two-phonon subtraction operations from an initial Gaussian state to a non-Gaussian state that has a bimodal quadrature probability distribution and then returns back to equilibrium. In Fig. 3(c), $\text{Pr}(X_m)$ is plotted at the time of the herald event where the non-Gaussianity generated is most significant. Note how the bimodal nature of the distribution is more distinct for the two-phonon subtracted state in comparison to the single-phonon subtracted case, in line with the theoretical prediction [49] overlayed.

Outlook.—Utilizing both photon counting and optical heterodyne measurements with a Brillouin optomechanics

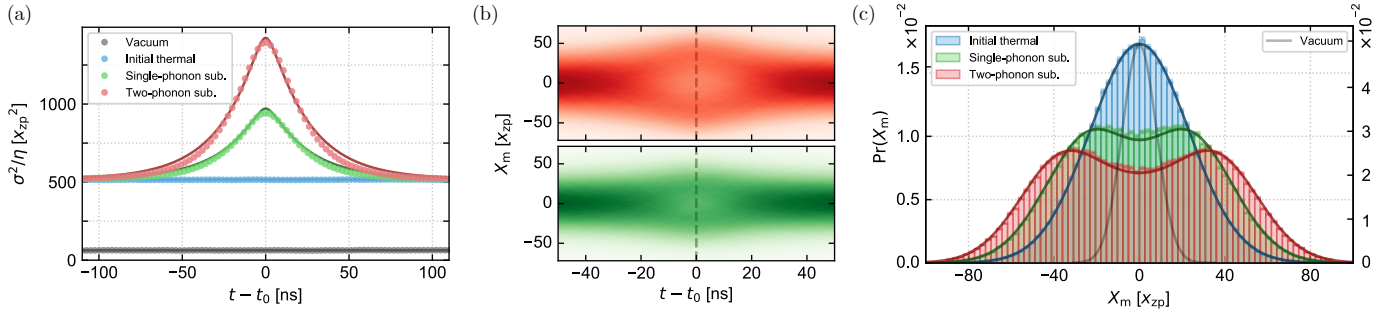


FIG. 3. Dynamics and non-Gaussian distributions of the heralded mechanical states. (a) Time evolution of the variance of the X_m quadrature in units of the mechanical zero-point fluctuations about the heralding event for single- and two-phonon subtracted thermal states, plotted in green and red, respectively. The optical vacuum is plotted in gray and the variance of the initial thermal state (zero subtractions) is plotted in blue. Experimental data is shown as dots, and the solid lines show expected evolution from theory. The theoretical model does not account for filtering in post-processing or dark counts from the SPADs, explaining the small discrepancy. At the time of the heralding event, the ratio of the heterodyne variance to the optical vacuum noise increases by a factor of 1.94 and 2.94 relative to the initial thermal state for single- and two-phonon subtraction, respectively. Marginal distributions for the X -quadrature of the mechanical oscillator as a function of time (b) and at the time of the heralding event, $t = t_0$, (c) for the initial (blue), single-phonon subtracted (green), and two-phonon subtracted (red) thermal mechanical states.

experiment, we report the generation and phase-space characterization of non-Gaussian states of mechanical motion via single- and two-phonon subtraction to a thermal state. This work makes key steps towards mechanical phase-space tomography of nonclassical mechanical states, which remains an outstanding goal within optomechanics. Furthermore, the techniques developed here can be utilized for a wide range of mechanical quantum state engineering applications taking advantage of single- and multiple-phonon addition and subtraction operations. In particular, these operations can be applied to a mechanical squeezed state for superposition state preparation [46], and reservoir engineering has been discussed as a promising route to generate the squeezing in such protocols [47, 48]. For this particular experiment, there are two key pathways for further studies and improvements. First, following a mechanical state preparation stage, a greater efficiency state readout can be performed by increasing the drive strength and utilizing the optomechanical strong coupling available for Brillouin optomechanics [45]. And, secondly, both the measurement efficiency and optomechanical cooperativity will be enhanced by operation at cryogenic temperatures where the mechanical decay rate will be greatly reduced [1–3]. Implement-

ing these two improvements provides a promising path to achieving an overall anti-Stokes readout measurement efficiency exceeding 50%. Achieving this efficiency, together with performing quantum-noise-limited time-domain homodyne detection, yields an s -parameter of $s > -1$, which is required to observe negativity of a quantum phase-space-distribution—a key signature of non-classicality and a powerful resource for quantum-enhanced technologies.

Note added.—During the preparation of this manuscript we became aware of related experimental work studying mechanical thermal states with a single added or subtracted phonon [50].

Acknowledgements.—We acknowledge useful discussions with P. Del’Haye, M. S. Kim, J. Nunn, N. Moroney, A. Rauschenbeutel, P. Schneeweiss, J. Silver, and S. Zhang. This project was supported by the Engineering and Physical Sciences Research Council (EP/T031271/1, EP/P510257/1), UK Research and Innovation (MR/S032924/1), the Royal Society, the Aker Scholarship, EU Horizon 2020 Program (847523 ‘INTERACTIONS’), and the Australian Research Council (CE170100012, FL150100019). (†) G.E., L.F., J.J.P., and A.Ø.S. contributed equally to this work and are listed alphabetically.

[1] S. Galliou, M. Goryachev, R. Bourquin, P. Abbe, J. P. Aubry, and M. E. Tobar, *Sci. Rep.* **3**, 2132 (2013).

[2] W. H. Renninger, P. Kharel, R. O. Behunin, and P. T. Rakich, *Nat. Phys.* **14**, 601 (2018).

[3] G. S. MacCabe *et al.*, *Science* **370**, 840 (2020).

[4] A. P. Higginbotham *et al.*, *Nat. Phys.* **14**, 1038 (2018).

[5] M. Mirhosseini *et al.*, *Nature* **588**, 599 (2020).

[6] P. H. Kim, B. D. Hauer, C. Doolin, F. Souris, and J. P. Davis, *Nat. Commun.* **7**, 13165 (2016).

[7] F. Monteiro, S. Ghosh, A. G. Fine, and D. C. Moore, *Phys. Rev. A* **96**, 063841 (2017).

[8] D. Carney, A. Hook, Z. Liu, J. M. Taylor, and Y. Zhao, New *J. Phys.* accepted, (2021) (arXiv:1908.04797).

[9] S. Bose, K. Jacobs, and P. L. Knight, *Phys. Rev. A* **59**, 3204 (1999).

[10] W. Marshall, C. Simon, R. Penrose, and D. Bouwmeester, *Phys. Rev. Lett.* **91**, 130401 (2003).

[11] A. Bassi, K. Lochan, S. Satin, T. P. Singh, and H. Ulbricht, *Rev. Mod. Phys.* **85**, 471 (2013).

[12] I. Pikovski *et al.*, *Nat. Phys.* **8**, 393 (2012).

[13] S. Bose *et al.*, *Phys. Rev. Lett.* **119**, 240401 (2017).

[14] C. Marletto and V. Vedral, *Phys. Rev. Lett.* **119**, 240402 (2017).

[15] D. Leibfried *et al.*, *Phys. Rev. Lett.* **77**, 4281 (1996).

[16] C. Flühmann *et al.*, *Nature* **566**, 513 (2019).

[17] A. I. Lvovsky *et al.*, *Phys. Rev. Lett.* **87**, 050402 (2001).

[18] A. Ourjoumtsev, R. Tualle-Brouri, J. Laurat, and P. Grangier, *Science* **312**, 83 (2006).

[19] J. S. Neergaard-Nielsen, B. Melholt Nielsen, C. Hettich, K. Molmer, and E. S. Polzik, *Phys. Rev. Lett.* **97**, 083604 (2006).

[20] T. Gerrits *et al.*, *Phys. Rev. A* **82**, 031802(R) (2010).

[21] A. Zavatta, V. Parigi, and M. Bellini, *Phys. Rev. A* **75**, 052106 (2007).

[22] V. Parigi, A. Zavatta, M. S. Kim, and M. Bellini, *Science* **317**, 1890 (2007).

[23] Yu. I. Bogdanov *et al.*, *Phys. Rev. A* **96**, 063803 (2017).

[24] S. Deleglise *et al.*, *Nature* **455**, 510 (2008).

[25] R. McConnell, H. Zhang, J. Hu, S. Cuk, and V. Vuletic, *Nature* **519**, 439 (2015).

[26] M. Hofheinz *et al.*, *Nature* **459**, 546 (2009).

[27] Y. Chu, P. Kharel, T. Yoon, L. Frunzio, P. T. Rakich, and R. J. Schoelkopf, *Nature* **563**, 666 (2018).

[28] K. J. Satzinger *et al.*, *Nature* **563**, 661 (2018).

[29] K. C. Lee *et al.*, *Nat. Photonics* **6**, 41 (2012).

[30] K. A. G. Fisher *et al.*, *Phys. Rev. A* **96**, 012324 (2017).

[31] S. T. Velez, *et al.*, *Phys. Rev. X* **9**, 041007 (2019).

[32] R. Riedinger *et al.*, *Nature* **530**, 313 (2016).

[33] J. D. Cohen *et al.*, *Nature* **520**, 522 (2015).

[34] I. Galinskiy, Y. Tsaturyan, M. Parniak, E. S. Polzik, *Optica* **7**, 718 (2020).

[35] G. Enzian *et al.*, *Phys. Rev. Lett.* **126**, 033601 (2021).

[36] M. R. Vanner, J. Hofer, G. D. Cole, and M. Aspelmeyer, *Nat. Commun.* **4**, 2295 (2013).

[37] J. T. Muonen, G. R. La Gala, R. Leijssen, and E. Verhagen, *Phys. Rev. Lett.* **123**, 113601 (2019).

[38] O. Suchoi, K. Shlomi, L. Ella, and E. Buks, *Phys. Rev. A* **91**, 043829 (2015).

[39] M. Rashid, M. Toros, and H. Ulbricht, *Quantum Meas. Quantum Metrol.* **4**, 17 (2017).

[40] M. Ringbauer *et al.*, *New J. Phys.* **20**, 053042 (2018).

[41] M. R. Vanner, I. Pikovski, and M. S. Kim, *Ann. Phys. (Berl.)* **527**, 15 (2015).

[42] M. R. Vanner, M. Aspelmeyer, and M. S. Kim, *Phys. Rev. Lett.* **110**, 010504 (2013).

[43] S. M. Barnett, G. Ferenczi, C. R. Gilson, and F. C. Speirits, *Phys. Rev. A* **98**, 013809 (2018).

[44] U. Leonhardt and H. Paul, *Phys. Rev. A* **48**, 4598 (1993); U. Leonhardt, ‘Measuring the Quantum State of Light’ Cambridge University Press (1997).

[45] G. Enzian *et al.*, *Optica* **6**, 7 (2019).

[46] T. J. Milburn, M. S. Kim, and M. R. Vanner, *Phys. Rev. A* **93**, 053818 (2016).

[47] I. Shomroni, L. Qiu, and T. J. Kippenberg, *Phys. Rev. A* **101**, 033812 (2020).

[48] H. Zhan, G. Li, and H. Tan, *Phys. Rev. A* **101**, 063834 (2020).

[49] See the Supplementary Material online for further details.

[50] R. N. Patel *et al.*, arXiv:2102.04017 (2021).

SUPPLEMENTARY MATERIAL

Non-Gaussian mechanical motion via single and multi-phonon subtraction from a thermal state

G. Enzian^{†,1,2,3} L. Freisem^{†,1,2} J. J. Price^{†,1,2} A. Ø. Svela^{†,1,2,4} J. Clarke,¹
B. Shajilal,⁵ J. Janousek,⁵ B. C. Buchler,⁵ P. K. Lam,⁵ M. R. Vanner^{1,2,*}

¹*QOLS, Blackett Laboratory, Imperial College London, London SW7 2BW, UK*

²*Clarendon Laboratory, Department of Physics, University of Oxford, Oxford OX1 3PU, UK*

³*Niels Bohr Institute, University of Copenhagen, Copenhagen 2100, Denmark*

⁴*Max Planck Institute for the Science of Light, Staudtstraße 2, 91058 Erlangen, Germany*

⁵*Centre for Quantum Computation and Communication Technology, Research School of Physics and Engineering, Australian National University, Canberra 2601, Australia*

A. Multi-phonon subtraction and addition to a thermal state

We consider an initial sideband-cooled thermal state $\rho_{\bar{n}}$ of a mechanical oscillator with mean occupation number \bar{n}

$$\rho_{\bar{n}} = \frac{1}{1 + \bar{n}} \sum_{m=0}^{\infty} \left(\frac{\bar{n}}{1 + \bar{n}} \right)^m |m\rangle\langle m| \quad (\text{S1})$$

$$= (1 - x) \sum_{m=0}^{\infty} x^m |m\rangle\langle m|. \quad (\text{S2})$$

Here, $x = \bar{n}/(1 + \bar{n})$. An n -phonon subtraction operation to $\rho_{\bar{n}}$ creates the state

$$\rho_{n-} = \frac{b^n \rho_{\bar{n}} b^{\dagger n}}{\text{Tr}(b^n \rho_{\bar{n}} b^{\dagger n})}, \quad (\text{S3})$$

while an n -phonon addition operation yields

$$\rho_{n+} = \frac{b^{\dagger n} \rho_{\bar{n}} b^n}{\text{Tr}(b^{\dagger n} \rho_{\bar{n}} b^n)}. \quad (\text{S4})$$

The mean phonon number of the n -phonon-subtracted state ρ_{n-} is given by

$$\langle b^{\dagger} b \rangle_{n-} = \frac{\text{Tr}(b^{n+1} \rho_{\bar{n}} b^{\dagger n+1})}{\text{Tr}(b^n \rho_{\bar{n}} b^{\dagger n})}. \quad (\text{S5})$$

Here, the trace terms $\text{Tr}(b^k \rho_{\bar{n}} b^{\dagger k})$ with $k \in \mathbb{N}$, may be calculated by using $b^k |m\rangle = \sqrt{m!/(m-k!)} |m-k\rangle$ for $m \geq k$ and $b^k |m\rangle = 0$ otherwise, to arrive at

$$\text{Tr}(b^k \rho_{\bar{n}} b^{\dagger k}) = (1 - x) \sum_{m=0}^{\infty} \frac{m!}{(m-k)!} x^m \quad (\text{S6})$$

$$= \frac{k!}{(1-x)^k} x^k. \quad (\text{S7})$$

This expression for the trace may be inserted into Eqs. (S3) and (S5) to give the explicit form of the density operator ρ_{n-} and the mean phonon number $\langle b^{\dagger} b \rangle_{n-}$

$$\rho_{n-} = \sum_{m=0}^{\infty} p_{n-}(m) |m\rangle\langle m|, \quad (\text{S8})$$

$$p_{n-}(m) = (1 - x)^{n+1} x^m \binom{m+n}{n}, \quad (\text{S9})$$

$$\langle b^{\dagger} b \rangle_{n-} = (n+1)\bar{n}. \quad (\text{S10})$$

A similar calculation allows one to calculate the density operator and the mean phonon number of the n -phonon-added state ρ_{n+} , which are given by

$$\rho_{n+} = \sum_{m=0}^{\infty} p_{n+}(m) |m\rangle\langle m|, \quad (\text{S11})$$

$$p_{n+}(m) = (1-x)^{n+1} x^{m-n} \binom{m}{n}, \quad (\text{S12})$$

$$\langle b^\dagger b \rangle_{n+} = (n+1)\bar{n} + n. \quad (\text{S13})$$

Here, the binomial coefficient $\binom{m}{n} = 0$ for $m < n$, such that phonon-number states $|m\rangle$ with $m < n$ of ρ_{n+} are unoccupied. This property also leads to the observation that the phonon-number distribution of ρ_{n+} and ρ_{n-} are equal up to a shift $p_{n+}(m) = p_{n-}(m-n)$. We also note that to further generalize these results, moment-generating functions are a valuable and elegant tool for these types of statistics [S. M. Barnett, G. Ferenczi, C. R. Gilson, and F. C. Speirits, *Phys. Rev. A* **98**, 013809 (2018)].

To further study the similarity of the states ρ_{n-} and ρ_{n+} we calculate the quantum state fidelity between them. By using $[\rho_{n-}, \rho_{n+}] = 0$, one has that the fidelity is $F(\rho_{n-}, \rho_{n+}) = \sum_m \sqrt{p_{n-}(m)p_{n+}(m)}$, which is strictly less than one. Utilizing $\binom{m+n}{n} < \binom{m}{n}$, we then derive a lower bound for the fidelity

$$\left(\frac{\bar{n}}{1+\bar{n}} \right)^{n/2} < F(\rho_{n-}, \rho_{n+}) < 1. \quad (\text{S14})$$

For finite n , this lower bound approaches one from below as \bar{n} increases, and hence we conclude that the two states are approximately the same in the high \bar{n} limit. Moreover, to arrive at a stringent condition on \bar{n} and n for the states ρ_{n-} and ρ_{n+} to be the same, we demand that the separation of the means $\langle b^\dagger b \rangle_{n+} - \langle b^\dagger b \rangle_{n-}$ is much less than the variance in phonon number $\text{Var}(\rho_{n+}, b^\dagger b) = \text{Var}(\rho_{n-}, b^\dagger b)$. This gives $\bar{n} \gg \left(-(1+n) + \sqrt{4n^3 + 5n^2 + 2n + 1} \right) / (2(1+n))$, where the right hand side of this inequality is an increasing function of n . Hence, at high values of n , we arrive at the condition for the mechanical state generated by an n -phonon subtraction to a thermal state to be the same as that generated by an n -phonon addition operation, namely $\bar{n} \gg \sqrt{n}$.

B. Marginal distributions

The optical equivalence theorem relates the Glauber–Sudarshan P function $P(\beta)$ of a quantum state to its density operator ρ through

$$\rho = \int d^2\beta P(\beta) |\beta\rangle\langle\beta|. \quad (\text{S15})$$

For example, the P function of $\rho_{\bar{n}}$ is given by $P_{\bar{n}}(\beta) = e^{-|\beta|^2/\bar{n}} / \pi \bar{n}$. Using Eq. (S3), one finds that the P function of ρ_{n-} is

$$P_{n-}(\beta) = \frac{1}{n! \bar{n}^n} |\beta|^{2n} P_{\bar{n}}(\beta). \quad (\text{S16})$$

Note that $P_{n-}(\beta)$ only depends on the magnitude of β , which demonstrates the rotational symmetry of the state in phase space.

We then calculate the position marginal of ρ_{n-} to be

$$\text{pr}_{n-}(X_m) = \int d^2\beta P_{n-}(\beta) |\langle X_m | \beta \rangle|^2 \quad (\text{S17})$$

$$= \frac{\exp\left(-\frac{X_m^2}{1+2\bar{n}}\right)}{n!\pi^{\frac{3}{2}}\sqrt{1+2\bar{n}}} \sum_{k=0}^n \sum_{l=0}^k \binom{n}{k} \binom{2k}{2l} \Gamma\left[n-k+\frac{1}{2}\right] \Gamma\left[l+\frac{1}{2}\right] X_m^{2(k-l)} \frac{(2\bar{n})^{k-l}}{(1+2\bar{n})^{2k-l}}. \quad (\text{S18})$$

Due to the rotational symmetry of the state, the probability marginals are invariant under the transformation $X_m \rightarrow X_m(\theta) = X_m \cos \theta + P_m \sin \theta$.

1. Inefficiencies in measurement

The total measurement efficiency η of the mechanical state includes mechanics-light transduction efficiency and optical detection efficiencies. An inefficient measurement of the mechanical state marginal $\text{pr}(X_m)$ is described by a beamsplitter model for loss

$$\text{pr}(X_m; \eta) = \frac{1}{\sqrt{\pi(1-\eta)}} \int_{-\infty}^{+\infty} dX' \text{pr}(X') \exp\left(-\frac{\eta}{1-\eta}(X' - X_m/\sqrt{\eta})^2\right), \quad (\text{S19})$$

where $\text{pr}(X_m; \eta)$ is the marginal of the optical field to be measured [U. Leonhardt, ‘Measuring the Quantum State of Light’ Cambridge University Press (1997)]. Inserting $\text{pr}_{n-}(X_m)$ into Eq. (S19) yields

$$\begin{aligned} \text{pr}_{n-}(X_m; \eta) &= \frac{\exp\left[-X_m^2 \left(\frac{1}{1-\eta} - \frac{B^2}{A}\right)\right]}{n!\pi^2\sqrt{(1+2\bar{n})(1-\eta)}A} \sum_{k=0}^n \sum_{l=0}^k \sum_{p=0}^{k-l} \binom{n}{k} \binom{2k}{2l} \binom{2(k-l)}{2p} \Gamma\left[n-k+\frac{1}{2}\right] \\ &\quad \Gamma\left[l+\frac{1}{2}\right] \Gamma\left[p+\frac{1}{2}\right] \left(\frac{BX_m}{A}\right)^{2(k-l-p)} \frac{(2\bar{n})^{k-l}}{(1+2\bar{n})^{2k-l}} A^{-p}, \end{aligned} \quad (\text{S20})$$

where $A = 1/(1+2\bar{n}) + \eta/(1-\eta)$ and $B = \sqrt{\eta}(1-\eta)$.

An equivalent expression to Eq.(S19), describing the effect of the beamsplitter model is given by the P -function transformation: $P'(\beta) = \frac{1}{\eta}P(\beta/\sqrt{\eta})$, where $P'(\beta)$ is the P function of the optical field to be measured. Using Eq. (S16), the P function of ρ_{n-} therefore transforms according to $P'_{n-}(\beta) = P_{n-}(\beta; \bar{n} \rightarrow \eta\bar{n})$, which is a simple rescaling of the initial mean phonon number of the thermal state. According to Eq. (S17), the effect of inefficient measurement on the marginal $\text{pr}_{n-}(X_m)$ is also to rescale \bar{n} in the same way: $\bar{n} \rightarrow \eta\bar{n}$. Hence, $\text{pr}_{n-}(X_m; \eta) = \text{pr}_{n-}(X_m; \bar{n} \rightarrow \eta\bar{n})$.

2. Heterodyne detection and the s -parameterized Wigner function

Heterodyne detection projects the optical state ρ entering the detector onto a coherent state $|\alpha\rangle$. An outcome $\alpha \in \mathbb{C}$ occurs with probability proportional to $\text{Tr}(|\alpha\rangle\langle\alpha|\rho) = \langle\alpha|\rho|\alpha\rangle$. Hence, as the Husimi- Q function is defined as $Q(\alpha) = \frac{1}{2\pi}\langle\alpha|\rho|\alpha\rangle$, heterodyne detection allows one to measure the Q function of the optical state ρ .

In the case of a perfect measurement of the mechanical state, $\eta = 1$, heterodyne detection measures the Q function of the mechanical state $Q(X_m, P_m)$. The marginals of the Q function are related to the mechanical state marginals $\text{pr}(X_m)$ via a convolution with a Gaussian

$$\text{pr}(X_m; s = -1) = \int dP_m Q(X_m, P_m) \quad (\text{S21})$$

$$= \frac{1}{\sqrt{\pi}} \int dX' \text{pr}(X') e^{-(X_m - X')^2}. \quad (\text{S22})$$

This equation is again phase-invariant and $s = -1$ refers to condition for the s -parameterized Wigner function $W_s(X_m, P_m)$ to equal the Q function.

However, in the case of inefficient measurement, $\eta < 1$, the s -parameterized Wigner function $W_s(X_m, P_m)$ transforms to $W'_{s'}(X_m, P_m)$ according to [U. Leonhardt and H. Paul, Phys. Rev. A **48**, 4598 (1993)]

$$W'_{s'}(X_m, P_m) = \frac{1}{\eta} W_s(X_m \eta^{-1/2}, P_m \eta^{-1/2}), \quad (\text{S23})$$

$$s = \frac{1}{\eta} (s' + \eta - 1). \quad (\text{S24})$$

In general, this process acts to smooth the quasiprobability distributions $s < s'$ and rescales the X_m and P_m coordinates. Therefore, inefficient heterodyne detection, $s' = -1$, measures an s -parameterized Wigner function of the mechanical state with $s = (\eta - 2)/\eta$.

3. Measured marginal distributions

Here, we derive an expression that relates the mechanical marginal distribution $\text{pr}(X_m)$ to the distribution measured via inefficient heterodyne detection $\text{Pr}(X_m)$. Using Eq. (S23) and setting $s = (\eta - 1)/\eta$, we find the marginal distribution $\text{Pr}(X_m)$ of the field measured by heterodyne is

$$\text{Pr}(X_m) = \int dP_m Q'(X_m, P_m) \quad (\text{S25})$$

$$= \frac{1}{\eta} \int dP_m W_s(X_m \eta^{-1/2}, P_m \eta^{-1/2}) \quad (\text{S26})$$

$$= \frac{1}{\sqrt{\eta}} \int dP W_s(X_m \eta^{-1/2}, P) \quad (\text{S27})$$

$$= \frac{1}{\sqrt{\pi|s|\eta}} \int dX' \text{pr}(X') e^{-|s|^{-1}(X' - X_m/\sqrt{\eta})^2}. \quad (\text{S28})$$

Where in the last line, we used the relation between the marginal distribution $\text{pr}(X_m)$ and the marginal of the s -parameterized Wigner function $\text{pr}(X_m; s)$:

$$\text{pr}(X_m; s) = \frac{1}{\sqrt{\pi|s|}} \int dX' \text{pr}(X') e^{-|s|^{-1}(X_m - X')^2}, \quad (\text{S29})$$

valid for $s < 0$.

As expected, a convolution of $\text{pr}(X_m; \eta)$ and the Gaussian in Eq. (S22) yields the same expression for $\text{Pr}(X_m)$. This observation allows one to arrive at the neat expression for the measured marginal of the n -phonon subtracted state

$$\text{Pr}_{n-}(X_m) = \frac{1}{\sqrt{\pi}} \int dX' \text{pr}_{n-}(X'; \eta) e^{-(X_m - X')^2} \quad (\text{S30})$$

$$= \frac{\exp\left(-\frac{X_m^2}{2(1+\eta\bar{n})}\right)}{n! \pi^2 \sqrt{2(1+\eta\bar{n})}} \sum_{k=0}^n \sum_{l=0}^k \sum_{r=0}^{k-l} \binom{n}{k} \binom{2k}{2l} \binom{2(k-l)}{2r} \Gamma\left[n - k + \frac{1}{2}\right] \Gamma\left[l + \frac{1}{2}\right] \Gamma\left[r + \frac{1}{2}\right] \\ X_m^{2(k-l-r)} \frac{(2\eta\bar{n})^{k-l}}{(1+2\eta\bar{n})^{l+r} [2(1+\eta\bar{n})]^{2(k-l)-r}}. \quad (\text{S31})$$

Where the gamma functions are given by

$$\Gamma\left[m + \frac{1}{2}\right] = \frac{(2m)!}{4^m m!} \sqrt{\pi} \quad (\text{S32})$$

for $m \in \mathbb{N}$. Explicitly, the measured marginal distributions of the thermal state $\rho_{\bar{n}}$, single-phonon subtracted state ρ_{1-} , and two-phonon subtracted state ρ_{2-} are

$$\text{Pr}_{\bar{n}}(X_m) = \frac{1}{\sqrt{2\pi(1+\eta\bar{n})}} \exp\left[-\frac{X_m^2}{2(1+\eta\bar{n})}\right], \quad (\text{S33})$$

$$\text{Pr}_{1-}(X_m) = \frac{1}{\sqrt{8\pi(1+\eta\bar{n})}} \exp\left[-\frac{X_m^2}{2(1+\eta\bar{n})}\right] \left(\frac{2+\eta\bar{n}}{1+\eta\bar{n}} + \frac{4\eta\bar{n}}{[2(1+\eta\bar{n})]^2} X_m^2\right), \quad (\text{S34})$$

$$\begin{aligned} \text{Pr}_{2-}(X_m) = \frac{1}{\sqrt{8\pi(1+\eta\bar{n})}} \exp\left[-\frac{X_m^2}{2(1+\eta\bar{n})}\right] \times \\ \left(\frac{8+8\eta\bar{n}+3(\eta\bar{n})^2}{4(1+\eta\bar{n})^2} + \frac{4\eta\bar{n}+(\eta\bar{n})^2}{2(1+\eta\bar{n})^3} X_m^2 + \frac{(2\eta\bar{n})^2}{[2(1+\eta\bar{n})]^4} X_m^4\right), \end{aligned} \quad (\text{S35})$$

which simplify to the marginals of the mechanical Q functions when $\eta = 1$.

The maxima for the measured distribution of single-phonon subtracted state $\text{Pr}_{1-}(X_m)$ occur at $X_m = \pm X_1$

$$X_1 = \sqrt{\frac{(1+\eta\bar{n})(\eta\bar{n}-2)}{\eta\bar{n}}} \quad (\text{S36})$$

Hence, the condition to produce the non-Gaussian ring shape, characterized by a dip at $X_m = 0$, is $\eta\bar{n} > 2$.

We now sketch how we relate the location of the maxima of $\text{Pr}_{1-}(X_m)$ to the radius at which the maxima occur in W_s . First, we consider the simple expression for the P function of the single-phonon subtracted state by choosing $n = 1$ in Eq. (S16). We find that the maxima of $P_{1-}(\beta)$ occur at a radius $\sqrt{2\bar{n}}$ from the origin. Integrating $P_{1-}(\beta)$ over one quadrature then gives an expression for marginal of this P function: $\text{pr}_{1-}(X_m; s = +1)$. The maxima of $\text{pr}_{1-}(X_m; s = +1)$ occur at $X_m = \pm\sqrt{\bar{n}}$. Hence, there is a factor of $\sqrt{2}$ difference between the distance of the maxima from the origin of $\text{pr}_{1-}(X_m; s = +1)$ and $P_{1-}(\beta)$. Second, we then use Eq. (S29) and a two-dimensional convolution from the P function to W_s , to show that this factor of $\sqrt{2}$ difference persists at the level of $\text{Pr}_{1-}(X_m)$ and W_s . Hence, for ρ_{1-} the maxima of $W_s(X_m, P_m)$ occur at a radius of $r_1 = \sqrt{2}X_1$.

The maxima for measured distribution of two-phonon subtracted state $\text{Pr}_{2-}(X_m)$ occur at $X_m = \pm X_2$

$$X_2 = \sqrt{\frac{1+\eta\bar{n}}{\eta\bar{n}}} \left[-4 + \eta\bar{n} + \sqrt{2(4 + (\eta\bar{n})^2)}\right]. \quad (\text{S37})$$

A similar calculation to the one sketched above gives that for ρ_{2-} the maxima of $W_s(X_m, P_m)$ occur at a radius $r_2 = \sqrt{2}X_2$. In this case, the condition for the maxima to exist is given by $\eta\bar{n} > -4 + 2\sqrt{6}$.

4. Normalization to mechanical zero-point fluctuations

To normalize the measured s -parameterized Wigner function $W_s(X_m, P_m)$ to units of zero-point fluctuations of the mechanical oscillator, we first measure the optical vacuum signal. Heterodyne measurement of the vacuum signal yields the Q function $Q_{\text{vac}}(\beta) = \frac{1}{2\pi}|\langle\beta|0\rangle|^2 = \frac{1}{2\pi}e^{-|\beta|^2}$. Therefore, the measured distribution is first normalized such that the variance of the measured distribution is equal to one, agreeing with the expression $Q_{\text{vac}}(\beta)$ as we have $\beta = (X + iP)/\sqrt{2}$.

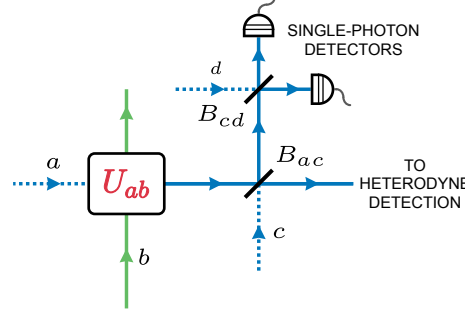


FIG. 4. Simplified schematic of the experimental setup used to implement and characterize two-phonon subtraction from a mechanical thermal state. Here, a represents the optical cavity mode of the scattered anti-Stokes signal, b is the mechanical mode, and U_{ab} is a unitary corresponding to a light-mechanics beamsplitter-like interaction. An auxiliary mode c has been introduced which participates in the optical beamsplitter, described by the unitary B_{ac} , dividing the light between the single-photon detectors and the heterodyne measurement.

Using Eq. (S28), and choosing $\text{pr}(X_m) = \text{pr}_{\bar{n}}(X_m)$, we have the measured distribution of the thermal state being

$$\text{Pr}_{\bar{n}}(X_m) = \frac{1}{\sqrt{\pi|s|\eta}} \int dX' \text{pr}_{\bar{n}}(X') e^{-|s|^{-1}(X' - X_m/\sqrt{\eta})^2}. \quad (\text{S38})$$

The variance of this measured thermal distribution is then given by

$$\sigma^2 = \eta \left(\bar{n} + \frac{1}{2} + \frac{1}{2}|s| \right), \quad (\text{S39})$$

with $s = (\eta - 2)/\eta$, such that as $\eta \rightarrow 0$, $\sigma^2 \rightarrow 1$, agreeing with the variance of the vacuum signal distribution. Inserting, $s = (\eta - 2)/\eta$ then gives

$$\sigma^2 = \eta\bar{n} + 1 \quad (\text{S40})$$

$$\eta = \frac{\sigma^2 - 1}{\bar{n}}. \quad (\text{S41})$$

The variance of the measured thermal distribution and knowledge of \bar{n} therefore allows one to determine η and s . Finally, to normalize to mechanical zero-point units we divide the quadrature axes, which have already been normalized to optical vacuum, by $\sqrt{\eta}$.

C. Temporal evolution of the heterodyne signal variance for two-phonon subtraction

In order to calculate the temporal evolution of the measured heterodyne signal variance for the case of two-phonon subtraction to a mechanical thermal state, we proceed in a similar manner to the calculation presented in the Supplementary Material of [Enzian *et al.*, Phys. Rev. Lett. **126**, 033601 (2021)] for the case of single-phonon subtraction.

Fig. 4 shows a simplified model of the joint click-dyne detection scheme considered. If the optical fields impinging on the single-photon detectors are weak, such that the probability of more than one photon arriving at a single detector (per gate duration) is negligible, the action of the detectors is well described by projection onto single-photon Fock states. For our scheme, this corresponds to the measurement operator

$$\Upsilon = \langle 1|_c \langle 1|_d B_{cd} |0\rangle_d B_{ac} |0\rangle_c \simeq \langle 2|_c B_{ac} |0\rangle_c \quad (\text{S42})$$

where B_{ac} and B_{cd} are beamsplitter unitaries between modes a and c , and c and d , respectively.

The mean quadrature variance of the optical cavity mode for a two-phonon subtracted thermal mechanical state is computed using

$$\langle X_{\text{cav}}^2(\tau) \rangle = \text{Tr}(\rho_c X_{\text{cav}}^2), \quad (\text{S43})$$

where ρ_c is the density operator of the conditioned state, given by

$$\rho_c = \frac{1}{\mathcal{P}} \langle 2|_c B_{\text{ac}} |0\rangle_c U_{\text{ab}} \rho_{\bar{n}} \otimes |0\rangle\langle 0|_a U_{\text{ab}}^\dagger \langle 0|_c B_{\text{ac}}^\dagger |2\rangle_c. \quad (\text{S44})$$

The normalization \mathcal{P} corresponds to the heralding probability, and $\rho_{\bar{n}} \otimes |0\rangle\langle 0|_a$ is the initial state of the whole system, where $\rho_{\bar{n}}$ is the density operator of the thermal mechanical state before the two-fold subtraction event, and $|0\rangle\langle 0|_a$ is the vacuum state of the optical cavity mode.

For a weak signal field arriving at the detectors, we take

$$B_{\text{ac}} \simeq 1 + ir(ac^\dagger + ca^\dagger) + r^2(ac^\dagger + ca^\dagger)^2/2 \quad (\text{S45})$$

where r is the amplitude reflectivity parameter of the optical beamsplitter, such that $\langle 2|_c B_{\text{ac}} |0\rangle_c = r^2 a^2/2$. Substituting this result into Eq. (S44), one obtains for the conditioned state

$$\rho_c = \frac{1}{\mathcal{P}} \left(\frac{r^2}{\sqrt{2}} \right)^2 a^2 U_{\text{ab}} \rho_{\bar{n}} \otimes |0\rangle\langle 0|_a U_{\text{ab}}^\dagger (a^\dagger)^2, \quad (\text{S46})$$

with the $\mathcal{P} = r^4 \langle (a^\dagger)^2 a^2 \rangle / 2$, such that the quadrature variance of the optical field is given by

$$\langle X_{\text{cav}}^2(\tau) \rangle = \frac{1}{\mathcal{P}} \left(\frac{r^2}{\sqrt{2}} \right)^2 \text{Tr}(\rho_{\bar{n}} \otimes |0\rangle\langle 0| U_{\text{ab}}^\dagger (a^\dagger)^2 X_{\text{cav}}^2 a^2 U_{\text{ab}}). \quad (\text{S47})$$

At this point, in order to capture the full cavity dynamics, solutions to the Heisenberg–Langevin equations of motion can be inserted into Eq. (S47) such that

$$\langle X_{\text{cav}}^2(\tau) \rangle = \frac{\langle a^\dagger(0)a^\dagger(0) X_{\text{cav}}^2(\tau) a(0)a(0) \rangle}{\langle a^\dagger(0)a^\dagger(0)a(0)a(0) \rangle^2}, \quad (\text{S48})$$

which, after inserting $X_{\text{cav}} = (a + a^\dagger)/\sqrt{2}$, and applying the commutation rules for the creation and annihilation operators of bosonic modes, becomes

$$\langle X_{\text{cav}}^2(\tau) \rangle = \frac{1}{2} + \frac{\langle a_0^\dagger a_0^\dagger a_\tau a_\tau^\dagger a_0 a_0 \rangle}{\langle a_0^\dagger a_0 \rangle^2}, \quad (\text{S49})$$

where we have introduced the notation $a_\tau \equiv a(\tau)$ for brevity, with $\tau = t - t_0 = 0$ denoting the heralding time of a two-phonon subtraction operation.

To proceed, the Isserlis–Wick theorem for Gaussian fields is applied to obtain

$$\langle a_0^\dagger a_0^\dagger a_\tau a_\tau^\dagger a_0 a_0 \rangle = 2 \langle a_0^\dagger a_0 \rangle^2 \langle a_\tau a_\tau^\dagger \rangle + 4 \langle a_0^\dagger a_0 \rangle |\langle a_0^\dagger a_\tau \rangle|^2, \quad (\text{S50})$$

such that

$$\langle X_{\text{cav}}^2(\tau) \rangle = \frac{1}{2} + \langle a_0^\dagger a_0 \rangle + \frac{2|\langle a_0^\dagger a_\tau \rangle|^2}{\langle a_0^\dagger a_0 \rangle}. \quad (\text{S51})$$

For a light-mechanics beamsplitter-like interaction, with Hamiltonian $H/\hbar = G(ab^\dagger + ba^\dagger)$, the solution to the Heisenberg–Langevin equation of motion for the optical cavity mode is given by Eq. (21) in the Supplementary Material of [Enzian *et al.*, Phys. Rev. Lett. **126**, 033601 (2021)] as

$$a(t) = \sqrt{2\kappa} \left(e^{-\kappa t} \Theta(t) \right) * a_{\text{in}}(t) - \frac{iG\sqrt{2\gamma}}{\kappa - \gamma} \left(\left(e^{-\gamma t} - e^{-\kappa t} \right) \Theta(t) \right) * b_{\text{in}}(t). \quad (\text{S52})$$

such that

$$\langle a_0^\dagger a_\tau \rangle = \frac{\bar{n}G^2}{\kappa(\kappa + \gamma)} \left(\frac{\kappa e^{-\gamma|\tau|} - \gamma e^{-\kappa|\tau|}}{\kappa - \gamma} \right) , \quad (\text{S53})$$

and

$$\langle a_0^\dagger a_0 \rangle = \frac{\bar{n}G^2}{\kappa(\kappa + \gamma)} . \quad (\text{S54})$$

Inserting the above correlations back into Eq. (S51), we obtain for the expected quadrature variance of the optical cavity mode for a two-phonon subtracted thermal mechanical state

$$\langle X_{\text{cav}}^2(\tau) \rangle = \frac{1}{2} + \frac{\bar{n}G^2}{\kappa(\kappa + \gamma)} \left(1 + 2 \left(\frac{\kappa e^{-\gamma|\tau|} - \gamma e^{-\kappa|\tau|}}{\kappa - \gamma} \right)^2 \right) . \quad (\text{S55})$$

Next, we note that in the experiment the measured signal is not the intra-cavity field but rather the output mode of the cavity. After accounting for this linear transformation, along with other losses in the system, we normalize such that variance of the optical vacuum is equal to 1, to arrive at

$$\sigma_{2-}^2(\tau) = 1 + \eta \bar{n} \left(1 + 2 \left(\frac{\kappa e^{-\gamma|\tau|} - \gamma e^{-\kappa|\tau|}}{\kappa - \gamma} \right)^2 \right) \quad (\text{S56})$$

for the measured heterodyne variance of a two-phonon subtracted thermal state, where η is the overall measurement efficiency. Similarly, for the case of single-phonon subtraction we also have (see [Enzian *et al.*, Phys. Rev. Lett. **126**, 033601 (2021)] for further details)

$$\sigma_{1-}^2(\tau) = 1 + \eta \bar{n} \left(1 + \left(\frac{\kappa e^{-\gamma|\tau|} - \gamma e^{-\kappa|\tau|}}{\kappa - \gamma} \right)^2 \right) . \quad (\text{S57})$$

Finally, Eqs. (S57) and (S56), can be rearranged to obtain the effective occupation of the single- and two-phonon subtracted thermal states about the heralding event, which, in units of the mechanical zero-point fluctuations, are given by

$$\bar{n}_{1-}(\tau) = \frac{\sigma_{1-}^2(\tau) - 1}{\eta} = \bar{n} \left(1 + \left(\frac{\kappa e^{-\gamma|\tau|} - \gamma e^{-\kappa|\tau|}}{\kappa - \gamma} \right)^2 \right) \quad (\text{S58})$$

and

$$\bar{n}_{2-}(\tau) = \frac{\sigma_{2-}^2(\tau) - 1}{\eta} = \bar{n} \left(1 + 2 \left(\frac{\kappa e^{-\gamma|\tau|} - \gamma e^{-\kappa|\tau|}}{\kappa - \gamma} \right)^2 \right) , \quad (\text{S59})$$

respectively.

From these results, it can be seen that at the time of the heralding event, the effective mechanical occupation doubles, $\bar{n}_{1-}(\tau = 0)/\bar{n} = 2$, and triples, $\bar{n}_{2-}(\tau = 0)/\bar{n} = 3$, for single- and two-phonon subtraction, respectively.

D. System characterization

To characterize our optomechanical system, we measure the spectrum of the thermally scattered anti-Stokes signal at a range of input powers. In the limit of weak coupling, it can be shown that the power spectral density of the scattered signal is given by

$$\begin{aligned} S_{XX}(\omega) &= \int_{-\infty}^{\infty} d\omega \langle \tilde{X}^\dagger(\omega) \tilde{X}(\omega) \rangle \\ &\propto |\chi_{\text{bb}}(\omega - \omega_H)|^2 + |\chi_{\text{bb}}(-\omega - \omega_H)|^2 , \end{aligned} \quad (\text{S60})$$

where \tilde{X} is the Fourier transform of the X -quadrature, ω_H is the heterodyne frequency, and

$$\chi_{bb}(\omega) = \frac{\sqrt{2\gamma}}{i\omega + \gamma_{\text{eff}}} \quad (\text{S61})$$

is the mechanical susceptibility in the limit of $\gamma \ll \kappa_2$. The effective mechanical amplitude decay rate is given by $\gamma_{\text{eff}} = \gamma(1 + C)$, where $C = G^2/\kappa_2\gamma$ is the optomechanical cooperativity.

In our experiment, we operate well within the weak-coupling regime and note that the intrinsic mechanical decay rate is much less than the decay rate of the “scattered into” anti-Stokes optical mode ($\gamma/\kappa \simeq 0.07$). The spectrum of the backscattered anti-Stokes signal is therefore well approximated by a Lorentzian function with a full-width half-maximum given by $2\gamma_{\text{eff}}$ that scales linearly with the number of intra-cavity pump photons.

The experimental setup used to measure the mechanical linewidth as a function of input power is the same as in Fig. 1 of the main text. To obtain the spectra of the scattered signal we Fourier-transform time traces from the output of the balanced heterodyne detector at each input power. To observe optomechanical broadening of the signal linewidth, the measurement is performed for input powers up to $\simeq 10$ mW, as shown in Fig. 5. Fitting to γ_{eff} , we obtain an intrinsic mechanical decay rate of $2\gamma/2\pi = 6.52(80)$ MHz, which is in good agreement with room-temperature Brillouin linewidths reported in similar materials [T. Sonehara *et al.*, J. Opt. Soc. Am. B **24**, 1193–1198 (2007)]. Furthermore, from the gradient we also obtain $g_0/2\pi = 296(37)$ Hz.

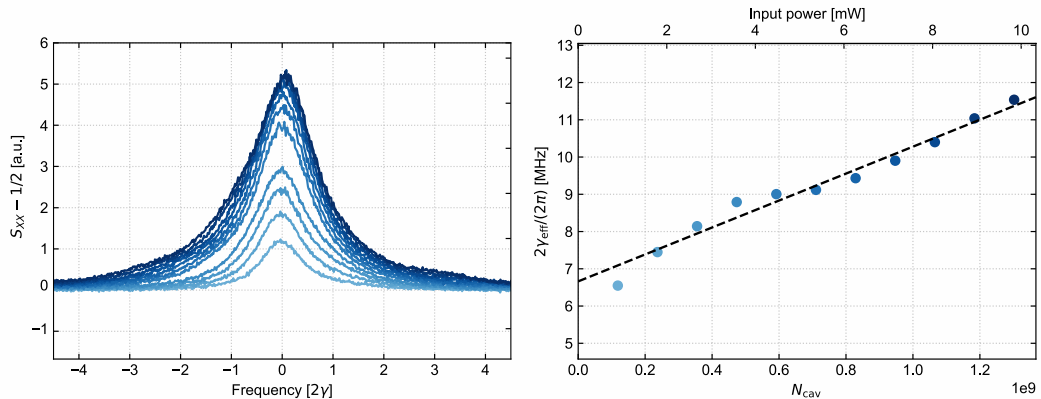


FIG. 5. (a) Mean spectrum of the thermally scattered anti-Stokes light at various input powers with frequency plotted in units of the intrinsic mechanical decay rate γ . Darker shades correspond to higher input powers up to a maximum of 10 mW. (b) Effective mechanical linewidth as a function of intra-cavity pump photon number with linear fit indicated by a dashed line.

The linewidths of the optical cavity modes are determined by sweeping the pump laser in frequency at low power. The pump and anti-Stokes optical resonances are measured to be $2\kappa_1/2\pi = 14.1$ MHz and $2\kappa_2/2\pi = 93.7$ MHz, respectively. Note that in order to compute the pump intra-cavity photon number we use $N_{\text{cav}} = \eta_{c,1}P_{\text{in}}/(\kappa_1\hbar\omega)$, where κ_1 is the (amplitude) decay rate of the optical pump mode and $\eta_{c,1} = 2\kappa_1^e/\kappa_1$. The extrinsic optical decay rate is calculated using $\kappa_1^e = \kappa_1(1 - \sqrt{T_0})/2$ where T_0 is the on-resonance transmission of the pump-mode (for under-coupled coupling conditions, as pertinent to this work).

Finally, we quantify the amount of optomechanical sideband-cooling that has occurred prior to the single and two-phonon subtraction events. In the limit of weak coupling, the effective mechanical occupancy in the steady-state is given by

$$\bar{n} = \frac{\bar{n}_{\text{th}}}{2\pi} \int_{-\infty}^{\infty} d\omega |\chi_{bb}(\omega)|^2 = \frac{\bar{n}_{\text{th}}}{1 + C} \quad (\text{S62})$$

where \bar{n}_{th} is the initial occupation of the mechanical mode in the absence of any optomechanical coupling and is given by $\bar{n}_{\text{th}} = k_{\text{b}}T/(\hbar\omega_{\text{m}})$ in the limit of high temperature T ($k_{\text{b}}T \gg \hbar\omega_{\text{m}}$), where k_{b} is the Boltzmann constant and ω_{m} is the angular frequency of the mechanical mode. For the 8.16 GHz acoustic wave used in this work we have $\bar{n}_{\text{th}} \simeq 766$. For $G/2\pi \simeq 10$ MHz, as described in the main text, the resulting steady-state occupancy of the unconditioned mechanical state is given by $\bar{n} = 453(52)$, corresponding to a sideband-cooling factor of $\simeq 0.6$.

E. Experimental system parameters

An overview of our system and experimental parameters can be found in Table I and Table II, respectively.

TABLE I. System parameters.

Parameter	Symbol	Value
Resonator major diameter	D_{res}	0.936 mm
Resonator minor radius	r_{res}	40 μm
Pump wavelength	λ_{p}	1550 nm
Mechanical frequency	$\omega_{\text{m}}/2\pi$	8.16 GHz
Mechanical linewidth	$2\gamma/2\pi$	6.52(80) MHz
Pump mode linewidth	$2\kappa_1/2\pi$	14.1 MHz
Pump mode external coupling	$2\kappa_1^{\text{e}}/2\pi$	5.3 MHz
Signal (aS) mode linewidth	$2\kappa_2/2\pi$	93.7 MHz
Signal (aS) mode external coupling	$2\kappa_2^{\text{e}}/2\pi$	11.7 MHz
Taper coupling efficiency (aS mode)	$\eta_{\text{c}} = 2\kappa_2^{\text{e}}/\kappa_2$	$\simeq 0.25$
Optomechanical coupling rate	$g_0/2\pi$	296(37) Hz
Intra-cavity pump photon number	N_{cav}	$\simeq 1.2 \times 10^9$
Pump-enhanced coupling rate	$G/2\pi$	10.3(13) MHz
Optomechanical cooperativity	C	0.69(19)
Mean initial phonon number	\bar{n}_{th}	766
Mean effective phonon number	$\bar{n} \rightarrow 2\bar{n}$, $3\bar{n}$	453(52) \rightarrow 906, 1359

TABLE II. Experimental parameters.

Parameter	Value
Sample temperature	300 K
Taper transmission	0.89
Overall measurement efficiency, η	1.54%
Input pump power	$\simeq 9$ mW
Filtering efficiency	0.15
SPAD quantum efficiency	0.125
SPAD gate rate	50 kHz
SPAD gate length	3.5 ns
SPAD dead time	18 μs
SPAD dark count rate	$\simeq 1 \text{ s}^{-1}$
Count rate	260(60) s^{-1}
Coincidence rate	$\simeq 2 \text{ s}^{-1}$
Heterodyne frequency, $\omega_{\text{het}}/2\pi$	214 MHz
Balanced detector bandwidth	$\simeq 400$ MHz
Recorded time trace length	4 μs
Number of time traces per operation	2.4×10^5